PERGAMON

Chaos, Solitons and Fractals 13 (2002) 95–107

CHAOS
SOLITONS & FRACTALS

www.elsevier.com/locate/chaos

Analysis of the dynamics of a realistic ecological model

Christophe Letellier [a,*], M.A. Aziz-Alaoui [b]

[a] *Université de Rouen, Place Emile Blondel, CORIA UMR 6614, 76821 Mont Saint-Aignan Cedex, France*
[b] *Département de Mathématiques, L.M., Fac. Sc. Tech., BP 540, 76058 Le Havre Cedex, France*

Accepted 18 October 2000

Abstract

A fairly realistic three-species food chain model based on the Leslie–Gower scheme is investigated by using tools borrowed from the nonlinear dynamical systems theory. It is observed that two co-existing attractors may be generated by this ecological model. A type-I intermittency is characterized and a homoclinic orbit is found. © 2001 Elsevier Science Ltd. All rights reserved.

1. Introduction

In general, studies of ecological models are devoted to the analysis of the existence and stability of equilibria or persistence of food chains. However, the most interesting properties of a dynamical system are the type of transients and the nature of the dynamical behaviors. Such an approach is particularly important when the asymptotic behavior of the system is chaotic.

Recent studies have shown that chaotic dynamics may play an important role in continuous time models for ecological systems. For instance, there is some evidences that the real time evolution of species involved in two or three food chains could be characterized by chaotic attractors as observed in many natural food chains [1–7]. Most of these studies are devoted to models of simple food webs with one or two species, or with three species based on Lotka–Volterra or Holling type schemes. On the contrary, this paper is focussed on a fairly realistic three-species food chain ecological model, using Lotka and Leslie-Gower schemes as studied in [7]. This model describes a prey population $\tilde{x}$ which serves as the only food for a predator $\tilde{y}$. This specialist predator $\tilde{y}$ is, in turn, the prey of a generalist predator $\tilde{z}$ which is assumed to reproduce mostly sexually.

A study of the bifurcation diagram is done when the self-growth rate for the prey $\tilde{x}$ is varied. The evolution of the periodic orbit spectrum is investigated and a topological characterization of the chaotic attractor is provided for the ecological model aforementioned. Indeed, in the last decade, several studies have discussed the structure of chaotic attractors in terms of templates to describe how trajectories in the phase space associated with the system are studied. The main idea behind such studies is that an attractor can be described by its population of periodic orbits, their related symbolic dynamics and their linking numbers [8–10]. Such an analysis can be applied for three-dimensional systems like the three-species food chain model studied here.

This paper is organized as follows. In Section 2, the model is briefly described. In Section 3, the dependence of the asymptotic behavior generated by the aforementioned model on the growth rate of prey $\tilde{x}$ is

* Corresponding author.
E-mail address: christophe.letellier@coria.fr (C. Letellier).

0960-0779/01/$ - see front matter
PII: S0960-0779(00)00239-3

investigated by using first-return maps and symbolic dynamics. An intermittent behavior is described and a homoclinic orbit is investigated. It is shown that, for some bifurcation parameter values, co-existing attractors can be observed. Finally, some remarks are confined in Section 4.

2. The three-species food chain model

A quite realistic model involving a three-species food chain is considered. A prey species $\tilde{x}$ serves as the only food for the predator $\tilde{y}$ which is itself predated by another predator $\tilde{z}$. A typical situation of such a scheme would involve rodents, snakes and peacocks [11]. Interaction between the specialist predator $\tilde{y}$ and its prey $\tilde{x}$ may be modeled by the Volterra scheme, i.e., predator population dies out exponentially in the absence of its prey. Nevertheless, for a more realistic model, the interaction between this predator $\tilde{y}$ and the generalist predator $\tilde{z}$ is rather modeled by the Leslie–Gower scheme where the loss in a predator population is proportional to the reciprocal of per capita availability of its most favorite food. A set of ordinary differential equations governing the above model is then given by [12]:

$$\begin{aligned}
\dot{\tilde{x}} &= a_1\tilde{x} - b_1\tilde{x}^2 - \frac{\omega_0\tilde{x}\tilde{y}}{\tilde{x}+d_0},\\
\dot{\tilde{y}} &= -a_2\tilde{y} + \frac{\omega_1\tilde{x}\tilde{y}}{\tilde{x}+d_1} - \frac{\omega_2\tilde{y}\tilde{z}}{\tilde{y}+d_2},\\
\dot{\tilde{z}} &= c_0\tilde{z}^2 - \frac{\omega_3\tilde{z}^2}{\tilde{y}+d_3},
\end{aligned} \tag{1}$$

where a_1 is the rate of the self-growth for prey $\tilde{x}$; a_2 measures the rate at which $\tilde{y}$ will die out when no $\tilde{x}$ remain; ω_i's are the maximum value which per capita rate can attain; d_0 and d_1 signify the extent to which environment provides protection to the prey $\tilde{x}$; b_1 measures the strength of competition among individuals of the species $\tilde{x}$; d_2 is the value of $\tilde{y}$ at which per capita removal rate of $\tilde{y}$ becomes $\omega_2/2$; d_3 represents the residual loss in $\tilde{z}$ population due to severe scarcity of its favorite food $\tilde{y}$; c_0 describes the growth rate of the generalist predator $\tilde{z}$ by sexual reproduction, the number of males and females being assumed to be equal.

The number of bifurcation parameters of this model may be reduced from 10 to 8 by using a scaling transformation reading as [7]

$$\begin{aligned}
x &= \frac{a_1}{b_1}\tilde{x},\\
y &= \frac{a_1^2}{b_1\omega_0}\tilde{y},\\
z &= \frac{a_1^3}{b_1\omega_0\omega_2}\tilde{z},\\
t &= \frac{\tilde{t}}{a_1}.
\end{aligned} \tag{2}$$

The rescaled system then becomes

$$\begin{aligned}
\dot{x} &= x(1-x) - \frac{xy}{x+a},\\
\dot{y} &= -by + \frac{cxy}{x+d} - \frac{yz}{y+e},\\
\dot{z} &= fz^2 - \frac{gz^2}{y+h},
\end{aligned} \tag{3}$$

where the bifurcation parameters are defined as:

$$\begin{aligned} a &= \frac{b_1 d_0}{a_1}, \quad e = \frac{d_2 \omega_0 b_1}{a_1^2}, \\ b &= \frac{a_2}{a_1}, \quad f = \frac{c_0 a_1^2}{b_1 \omega_0 \omega_2}, \\ c &= \frac{\omega_1}{a_1}, \quad g = \frac{\omega_3}{\omega_2}, \\ d &= \frac{b_1 d_1}{a_1}, \quad h = \frac{d_3 \omega_0 b_1}{a_1^2}. \end{aligned} \tag{4}$$

In this study, the bifurcation parameters are set in such a manner so as they correspond to a realistic scheme [12,13]. They read as:

$$\begin{aligned} &a_2 = 1.0, \quad d_1 = 10.0, \quad \omega_0 = 1.0, \quad \omega_3 = 1.0, \\ &b_1 = 0.06, \quad d_2 = 10.0, \quad \omega_1 = 2.0, \quad c_0 = 0.03, \\ &d_0 = 10.0, \quad d_3 = 20.0, \quad \omega_2 = 0.405. \end{aligned} \tag{5}$$

The parameter values are chosen on the basis of previous studies [12] and correspond to quantitative measures of attributes of the rodent–snake–peacock food chain. The a_1-bifurcation parameter will be varied during the present analysis. The system (3) has six fixed points. One of them, F_0, is located at the origin of the phase space $\mathbb{R}^3(x,y,z)$. The others are:

$$F_1 = \begin{vmatrix} x_1 = 1 \\ y_1 = 0 \\ z_1 = 0 \end{vmatrix}, \quad F_2 = \begin{vmatrix} x_2 = 0 \\ y_2 = \frac{g}{f} - h \\ z_2 = b\left(h - e - \frac{g}{f}\right) \end{vmatrix}, \quad F_3 = \begin{vmatrix} x_3 = \frac{bd}{c-b} \\ y_3 = (1 - x_3)(a + x_3) \\ z_3 = 0 \end{vmatrix},$$

$$F_{4\pm} = \begin{vmatrix} x_{4\pm} = \frac{1-a}{2} \pm \sqrt{\frac{(a+1)^2}{4} - \frac{g}{f} + h}, \\ y_{4\pm} = \frac{g}{f} - h, \\ z_{4\pm} = \left(h - e - \frac{g}{f}\right)\left(b - \frac{x_{4\pm} c}{x_{4\pm} + d}\right). \end{vmatrix} \tag{6}$$

These six fixed points are located on the xy-plane projection for $a_1 = 1.93$ with a chaotic trajectory (Fig. 1). Fixed points F_0 and F_1 always exist. It may be shown that F_2 never exists in the positive octant [7]. The existence of the fixed points $F_{4\pm}$ have been studied by investigating their local and global stability [7]. Since, for the parameters given in (5), it is located in the positive octant, the fixed point F_3 will be designated as the 'inner fixed point'.

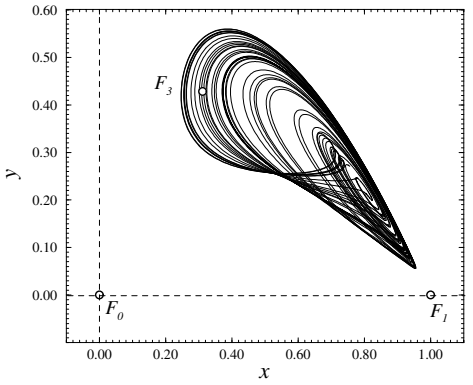

Fig. 1. Plane projection of the chaotic attractor observed for $a_1 = 1.93$. Three fixed points are also reported. F_2 is located very far from the attractor and not in the positive octant. The fixed points $F_{4\pm}$ are imaginary. None of the latter play any role in the dynamics.

3. Dynamical analysis

3.1. Bifurcation diagram and intermittent behavior

The asymptotic behavior settles down onto a chaotic attractor for $a_1 = 1.93$ whose plane projection is displayed in Fig. 1. A dynamical analysis of such a system starts by defining a Poincaré section as follows:

$$P_x \equiv \{(y_n, z_n) \in \mathbb{R}^2 \,|\, x_n = 0.80, \dot{x}_n < 0\}. \tag{7}$$

A bifurcation diagram is then computed. The a_1-bifurcation parameter is varied on the range [1.6; 3.6] (Fig. 2). A period-doubling cascade is observed. After the accumulation point, the behavior settles down onto a chaotic attractor which is structured on a skeleton of periodic orbits [14]. When the a_1-bifurcation parameter is increased, this skeleton is developed, i.e., new periodic orbits are created. Typically, two different bifurcations are involved. First, period-doubling bifurcations are easily identified in the main period-doubling cascade but also within each periodic window. Second, saddle-node bifurcations, creating one stable limit cycle and one unstable periodic orbit, both having the same period, may be identified at the beginning of each periodic window. One of them will be extensively studied in this section.

As predicted by the kneading theory [15], chaotic attractors observed just beyond the accumulation point of the period-doubling cascade are characterized by a unimodal first-return map, i.e., a map constituted by two monotonic branches separated by a critical point C_1 located at the differentiable maximum of the map (Fig. 3(a)). The first-return map remains unimodal while a_1 is less than 1.86560. Beyond this value, a third branch appears and the dynamics becomes bimodal (Fig. 3(b)). It is found that the dynamics remains bimodal for $a_1 \in [1.86560; 1.97740]$. A fourth monotonic branch then occurs after a tangent bifurcation associated with a saddle-node bifurcation creating two period-1 orbits (Fig. 3(c)) as observed on the Rössler system [10]. Since the period p of the orbits created is small ($p = 1$), a periodic window is easily observed (Fig. 2).

As usual, an intermittent behavior is observed before the periodic window. It results from a tangent bifurcation associated with the saddle-node bifurcation. In order to avoid numerical difficulties in computing the Poincaré section, the first-return map (Fig. 3(c)) is computed in the Poincaré section, defined as

$$P_z = \{(X_n, Z_n) \in \mathbb{R}^2 \,|\, Y_n = 0, Z_n > 0\},$$

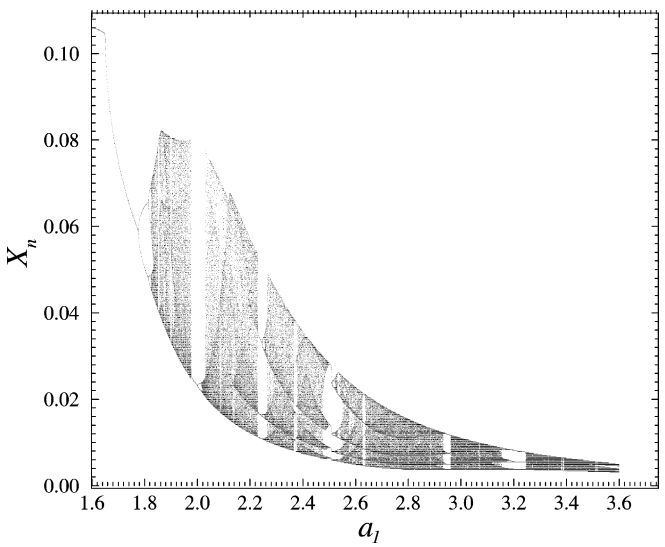

Fig. 2. The bifurcation diagram versus the a_1-control parameter of the ecological model for $c_3 = 0.03$.

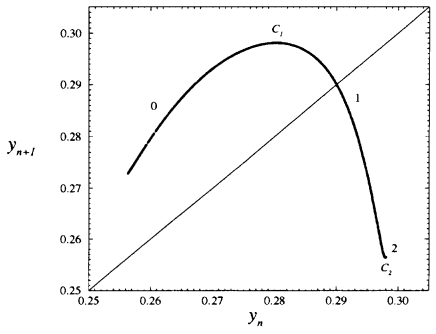

(a) $a_1 = 1.8660$

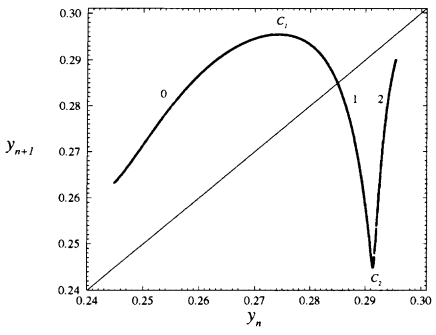

(b) $a_1 = 1.93$

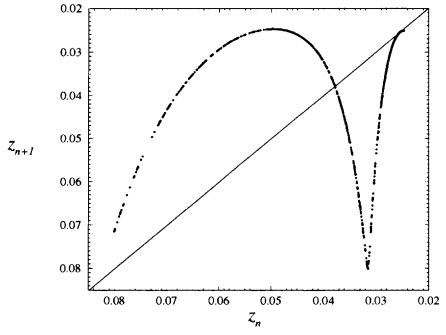

(c) $a_1 = 1.977403$

Fig. 3. First-return maps to the Poincaré section for different values of the bifurcation parameter a_1. A unimodal map with a differentiable maximum is found after the accumulation point as predicted by the kneading theory. For large a_1-values, a bimodal map is observed up to a tangent bifurcation for $a_1 = 1.977403$. (a) $a_1 = 1.8660$; (b) $a_1 = 1.93$; (c) $a_1 = 1.977403$.

where $X = z$, $Y = \dot{z}$ and $Z = \ddot{z}$, i.e., in the differential space induced by the z-time series. Such an induced space allows to avoid spurious intersections between the chaotic trajectory and the plane used to compute the Poincaré section. The first-return map is found to be tangent to the bissecting line for $a_1 = 1.97740$. Beyond, the asymptotic behavior settles down onto the period-1 limit cycle which is encoded by the orbital sequence (3), i.e., whose intersection with the Poincaré section is located on the fourth monotonic branch. Before the bifurcation, a thin canal between the first-return map and the bisecting line can be found. When the trajectory visits it, it stays for a long time very close to the limit cycle which will be created when the first-return map will reach the bissecting line. Thus, it seems that the trajectory travels on a periodic orbit during a significant time interval. When the trajectory escapes from this thin canal, it evolves on the chaotic attractor and a chaotic burst is observed (Fig. 4). Consequently, the intermittent behavior is characterized by the so-called laminar phases, during which the behavior is almost periodic for a finite time, interrupted by chaotic bursts before being reinjected in the thin canal. Such a scenario has been theoretically predicted by Pomeau and Manneville [16].

At least three types of intermittency exist, each of them being associated with a specific reinjection mechanism. They are distinguished by the distribution $P(l)$ of the laminar length l. Such a distribution computed for the intermittency just before the period-1 window is displayed in Fig. 5. It exhibits two characteristic lengths, one around 1000 s which is associated with the short phases while the other is around 4000 s and is associated with the long laminar phases. The diagram of the distribution of the laminar lengths is characteristic of a type-I intermittency [17] as expected when a saddle-node bifurcation is involved.

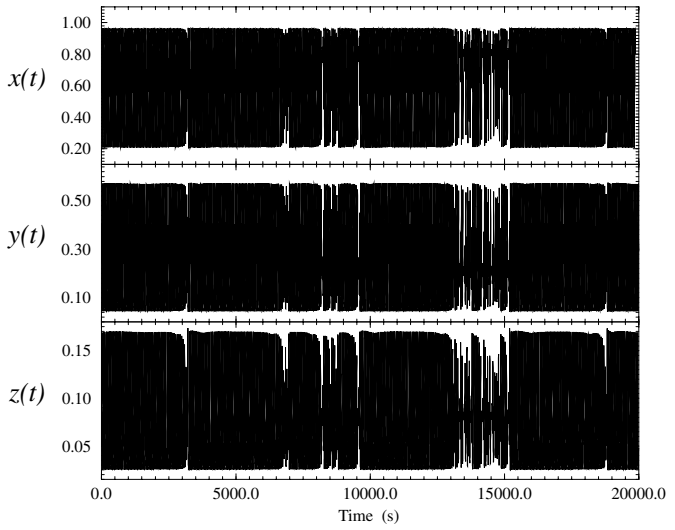

Fig. 4. Intermittent behavior is observed for $a_1 = 1.97740$. Laminar phases during which the behavior is almost periodic are interrupted by chaotic bursts ($c_0 = 0.03$).

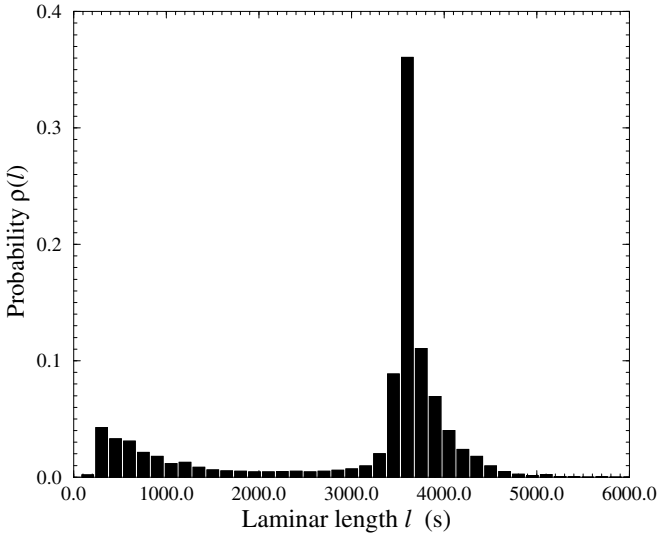

Fig. 5. Distribution of the laminar length l for $a_1 = 1.97740$ and $c_3 = 0.03$. The histogram is characteristic of a type-I intermittency.

3.2. Evolution of the orbit spectrum

The critical point C_i identified on the first-return map allows to define a partition of the attractor. Thus, each monotonic branch may be associated with a symbol to define a symbolic dynamics. For instance, when $a_1 \in [1.85653; 1.97740]$, the first-return map is constituted by three monotonic branches separated by two critical points, C_1 and C_2 (Fig. 3(b)). Any chaotic trajectory is then represented by a string of coordinates $\{y_n\}$ in the Poincaré section which is encoded by a string of symbols $\{\sigma_n\}$. Each symbol σ_n is defined according to the generating partition:

$$\sigma_n = \begin{cases} 0 & \text{if } y_n < C_1, \\ 1 & \text{if } C_1 < y_n < C_2, \\ 2 & \text{if } C_2 < y_n. \end{cases} \tag{8}$$

Such a symbolic dynamics then allows each periodic orbit embedded within the chaotic attractor by an orbital sequence [15,18] to be identified. In our case, the population of periodic orbits extracted from the chaotic attractor is reported in Table 1 for two values of a_1.

While the first-return map is unimodal with a differentiable maximum, the dynamics belongs to the universal class identified by Feigenbaum [19] and, independently, by Coullet and Tresser [20]. The evolution of the periodic orbit spectrum when the a_1-bifurcation parameter is varied is then well predicted by the unimodal forcing order [15,18]. Nevertheless, once a second critical point occurs, the dynamics is no longer unimodal and there is no universal order to predict the evolution of the orbit spectrum when a bifurcation parameter is varied [21]. Indeed, once two critical points are involved, two kinds of bifurcation may be involved, e.g., supercritical bifurcations increasing the number of periodic orbits and subcritical bifurcations decreasing the number of periodic orbits. When two critical points are identified, it often appears that one is associated with the supercritical bifurcations and the other with the subcritical bifurcations [22]. This is the case for the Rössler system. Such a concomitance has been called *antimonotonicity* by Dawson et al. [23].

When the orbit spectra extracted for $a_1 = 1.85653$ and $a_1 = 1.93$ are compared, it is remarked that there are some periodic orbits which are destroyed as exemplified by the four orbits encoded by $(10010), (10011), (20011)$ and (20010). As observed on the Rössler system [24,26], these orbits should be destroyed by inverse saddle-node bifurcations as displayed in Fig. 6(a). In each case, a stable limit cycle, (10011) or (20010), induces a period-doubling cascade. Such a destruction process results from

Table 1
Population of periodic orbits embedded within the attractor for two values of the a_1 bifurcation parameter ($c_0 = 0.03$)

(a) $a_1 = 1.8660$		(b) $a_1 = 1.93$			
(S)	(S)	(S)	(S)	(S)	(S)
1	10010	1	201	21100	211
10	10011	10	20110	21101	210
1011	20011	1011	20111	211011	210211
101110	20010	10110	201110	211020	21021
101111	200101	101	20100	211021	21020
10111	200100	100	20200	2110	210201
10110		100101	20	21110	21010
101		200101	21	211100	21011
100		200100	21201	21120	2111
100101		200	21200	21121	211121

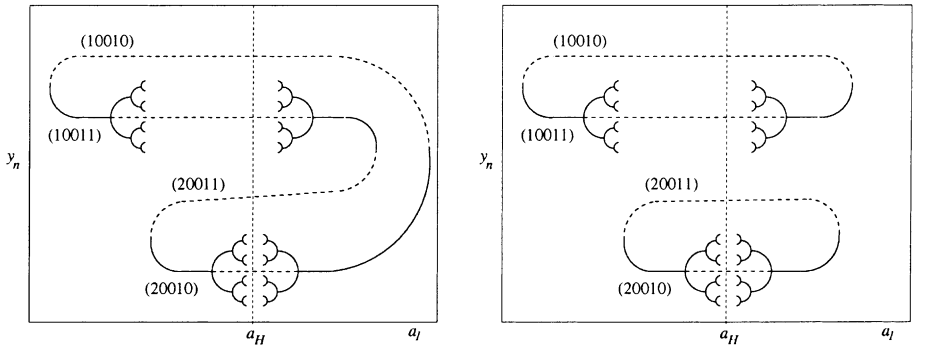

(a) Rössler system (b) Ecological model

Fig. 6. Mechanisms responsible for the destruction of the periodic orbits. The periodic orbits are created by two saddle-node bifurcations through the critical point C_1. In the case of the Rössler system, the orbit (20011) is destroyed with the orbit (10011) and (20010) with (10010). This feature comes from the fact that the destruction is governed by the critical point C_2. Contrary to this, in the case of the ecological model, the critical point C_2 has a very limited role and the destruction of the orbits is induced by the critical point C_1. Consequently, the orbit (10011) is destroyed with the orbit (10010), and (20011) with (20010). (a) Rössler system. (b) Ecological model.

the existence of a homoclinic orbit as observed on the Rössler system [10,24,25]. Once the homoclinic orbit is created for $a_1 = a_H$ (see Section 3.3), a destruction is involved by an inverse saddle-node bifurcation. In the case of the Rössler system, the inverse bifurcations are induced through the second critical point C_2. Contrary to this, in the case of the realistic ecological model, the periodic orbits are destroyed by inverse bifurcations involving the same pairs of orbits as involved in the creation process (Fig. 6(b)). It means that the second critical point C_2 has a weak role in the evolution of the orbit spectrum when a bifurcation parameter is varied and all the bifurcations (supercritical and subcritical) are induced by the critical point C_1 (for $a_1 < 1.97740$). The fact that the critical point C_1 is responsible for the creation as well as the desctruction induces that the third monotonic branch labelled '2' is quickly truncated as observed for $a_1 = 2.10$ (Fig. 7(a)). Such a feature is not observed on the Rössler system.

For higher a_1-values, i.e., $a_1 > 3.02$ (Fig. 7(c)), the first-return map is unimodal again, with a differentiable maximum. Consequently, the unimodal forcing order can be used to predict the evolution of the bifurcation diagram. In fact, when a_1 is increased beyond 3.02, inverse bifurcations are observed. It means that the periodic orbits embedded within the attractor become less numerous. The bifurcation diagram is therefore ended by a cascade of inverse period-doubling bifurcations.

When $a_1 \in]2.10; 3.02[$, it is rather difficult to compute a safe Poincaré section, i.e., without any spurious intersections between the trajectory and the Poincaré plane. These difficulties arise from the fact that there is no plane projection where a hole may be found in the middle of the attractor. As a consequence, spurious intersections cannot be avoided. For instance, for $a_1 = 2.20$ (Fig. 7(b)), a piece of a monotonic branch is observed near the bissecting line and located at the right side of the first-return map. Such a small branch is supicious. For these reasons, it may be difficult to describe the pruning process for periodic orbits. Nevertheless, up to five monotonic branches could be possibly identified on this range of a_1-values.

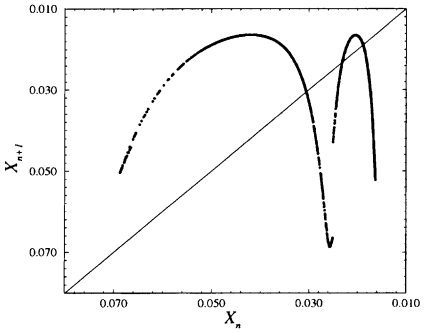

(a) $a_1 = 2.10$

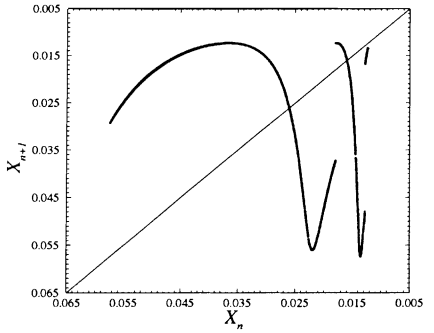

(b) $a_1 = 2.20$

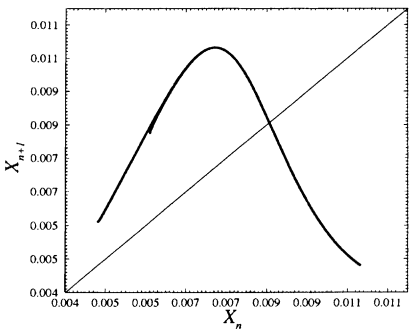

(c) $a_1 = 3.02$

Fig. 7. First-return maps to the Poincaré section P_z for three different high bifurcation parameter values. (a) $a_1 = 2.10$; (b) $a_1 = 2.20$; (c) $a_1 = 3.02$.

3.3. Multistability

When more than one critical points are identified, it may appear that two bifurcations involving low periodic orbits induce simultaneously a periodic window. In such a case, two co-existing stable limit cycles may be observed [22]. In the present case, the most observable periodic windows are the one associated with the main period-doubling cascade and the one associated with the saddle-node bifurcation inducing the stable period-1 limit cycle encoded by (3), i.e., corresponding to the intersection of the branch labelled by '3' with the bissecting line. When $c_0 = 0.03$, two second periodic windows are observed for very different values of a_1. Nevertheless, when the growth rate of the generalist predator c_0 is slightly increased, the saddle-node bifurcation appears for a_1-values sufficiently small to allow a co-existence of the stable limit cycle (3) with the main period-doubling cascade (Fig. 9). Indeed, the occurrence of the saddle-node bifurcation depends on the c_0-bifurcation parameter as displayed in Fig. 8. While a slight dependence on the c_0-value is observed for the period-doubling bifurcation inducing the period-8 limit cycle, increasing the growth rate of the general predator provokes an earlier saddle-node bifurcation inducing a couple of periodic orbits encoded by (2) and (3). Nevertheless, the bistability is observed for c_0 values a little bit larger than 0.036. For smaller values, only a periodic window is observed, i.e., the asympotic behavior is the period-1 limit cycle (3) for any initial conditions.

Thus, it has been observed that two attractors may co-exist, i.e., there are two attraction basins from which the asymptotic behavior settles down onto two different attractors. Such multistability is observed when the rate of the self-growth a_1 for prey x is varied on the interval [1.7804; 1.8915] (see Fig. 9). This feature is particularly important when an epidemic arises. For instance, when only one single attractor is observed, the sudden, widespread occurrence of an infectious disease in a community at a particular time induces a fast decrease of the population but, once the epidemic is finished, the population grows again up to the previous value and restarts to evolve with the same dynamics as the one observed before. Contrary to this, when two attractors co-exist, the epidemic may induce a transition from one attraction basin to the other and, consequently, the dynamical behavior after the disease may be different from the one observed before. Thus, an epidemic may affect deeply the equilibrium between different species.

In the present case, the two attractors are observed from the initial conditions

$$\begin{aligned} x_0 &= 1.2, & x_0 &= 0.2, \\ y_0 &= 1.2, \quad \text{and} & y_0 &= 0.2, \\ z_0 &= 1.2, & z_0 &= 0.2, \end{aligned}$$

respectively. For instance, for $a_1 = 0.17924$, a period-1 limit cycle coexists with a period-8 limit cycle (Fig. 10).

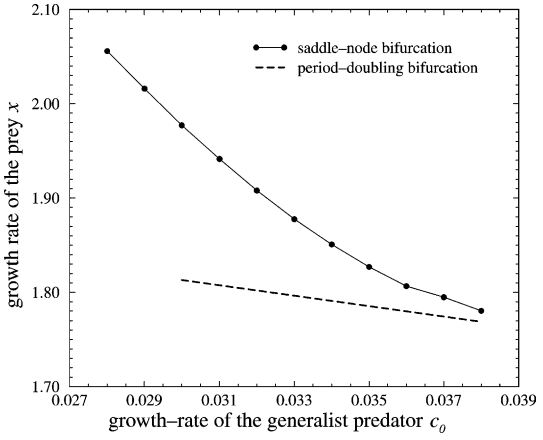

Fig. 8. When the growth-rate of the generalist predator c_0 is increased, the saddle-node bifurcation creating the stable limit cycle (3) and the unstable one (2) occurs for smaller values of the self-growth rate of the prey $\tilde{x}$. The period-doubling bifurcation inducing the period-8 limit cycle encoded by (10111010) is slightly dependent on c_0.

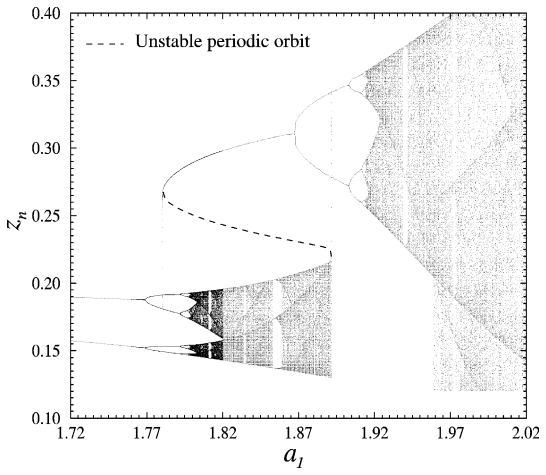

Fig. 9. Bifurcations diagram of the three-species food chain model for $c_0 = 0.038$. Two different attractors are observed when $a_1 \in [1.7804; 1.8915]$. Two co-existing period-doubling cascades are then observed. The chaotic attractor issued from the main one is destroyed by a boundary crisis with the unstable periodic orbit (2) created by the saddle-node bifurcation observed for $a_1 = 1.7804$. The stable limit cycle (3) is destabilized through a period-doubling bifurcation followed by a period-doubling cascade for $a_1 = 2.002$.

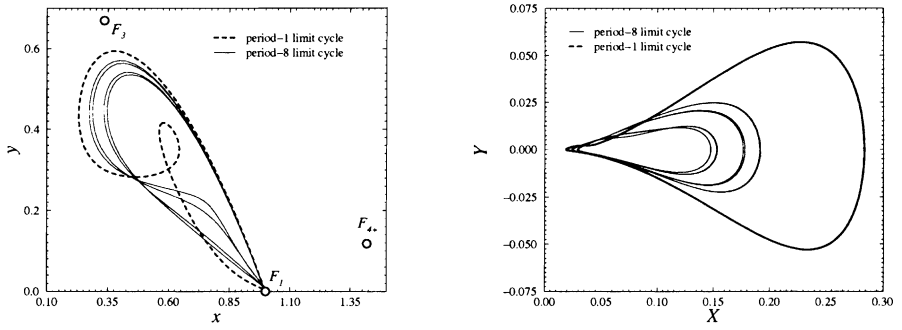

(a) xy-plane projection (b) XY-plane projection

Fig. 10. The period-1 limit cycle (3) coexists with the period-8 limit (10111010) cycle for $a_1 = 1.7924$. The small loop presented by the cycle (3) results from a projection effect and the limit cycle has rather a period equal to 1 as observed on the bifurcation diagram. For instance, another plane projection induced by the z-time series clearly confirms the periodicity of the limit cycle (3). This plane projection also exhibits that the stable limit cycle has a period equal to 8 rather than 4 as suggested by the xy-plane projection. They are involved in two different period-doubling cascades which are concomitant ($c_0 = 0.038$). (a) xy-plane projection. (b) XY-plane projection.

Let us remark that two stable limit cycles may co-exist for $c_3 = 0.03$ when the bifurcation parameter a_1 is set to 2.5. In such a case, a period-1 limit cycle coexists with a period-2 limit cycle (Fig. 11). Such a bistability explains the shift observed within the periodic window of the bifurcation diagram located at $a_1 = 2.5$ (Fig. 2).

3.4. Homoclinic orbit

When the growth-rate of the generalist predator $\tilde{z}$ is increased, it is observed that the saddle-node bifurcation is created for smaller values of the self-growth rate of the prey $\tilde{x}$. Contrary to this, by decreasing the c_0-bifurcation parameter, this saddle-node bifurcation occurs for larger values of a_1. In the same manner, the third monotonic branch of the first-return map appears later and, consequently, the unimodal map is more developed, i.e., orbital sequences of periodic orbits embedded within the attractor are

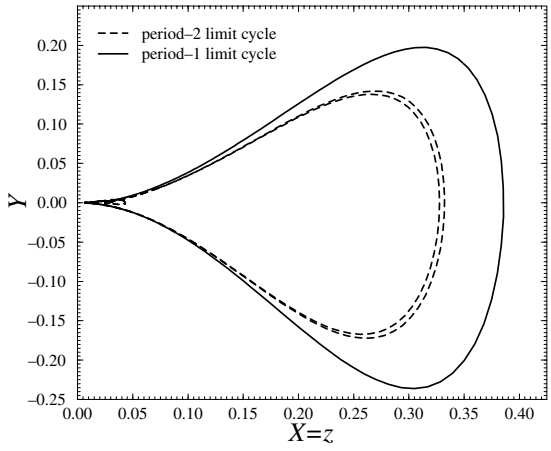

Fig. 11. Two co-existing limit cycles for $c_3 = 0.03$.

constituted by substring '0^n' with larger n. On the other hand, the increasing branch starts closer to the bisecting line.

Such a feature is particularly important since very often, as observed on the Rössler system [10], when the increasing branch reaches the bisecting line, a homoclinic orbit may be observed. A homoclinic orbit visits the small neighborhood of an inner fixed point, spaces out by its unstable manifold and is reinjected in the neighborhood of the same fixed point by its stable manifold. An existence criterion has been proposed by Sil'nikov [27]. A homoclinic orbit has been observed for $c_0 = 0.029101$ and $a_1 = 1.917420$ (Fig. 12(a)). It is checked that the increasing branch of the unimodal first-return map then reaches the bissecting line (Fig. 12(b)) as expected. In the present case, the trajectory visits a neighborhood where the derivatives become very small but, surprisingly, no fixed point has been identified in this neighborhood. For instance, the trajectory visits the point P which has the coordinates

$$\begin{aligned} x &= 0.795345, \\ y &= 0.160453, \\ z &= 0.073065, \end{aligned} \tag{9}$$

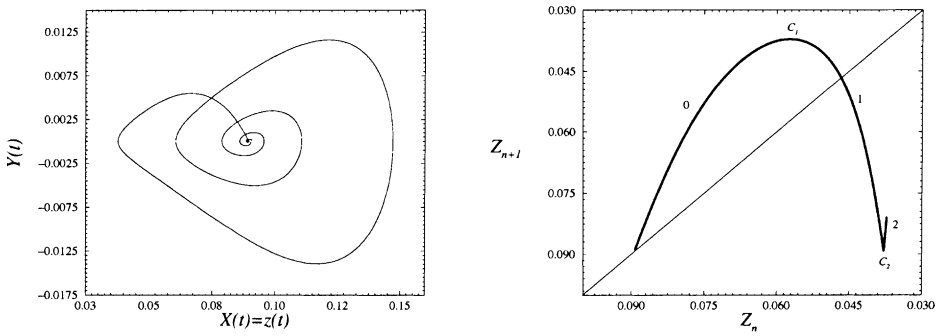

(a) XY-plane projection (b) First-return map

Fig. 12. An approximation of the homoclinic orbit observed on the three-species food chain model for $a_1 = 1.917420$ and $c_0 = 0.029101$. The trajectory visits the neighborhood of the inner fixed point F_{4+}. The first-return map exhibits an increasing branch which reaches the bisecting line. (a) XY-plane projection. (b) First-return map.

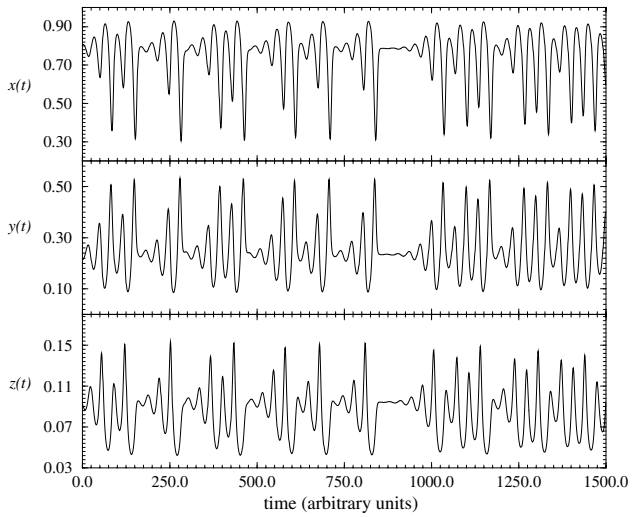

Fig. 13. Time evolution of the different normalized species in a homoclinic situation ($a_1 = 1.917420$ and $c_0 = 0.029101$).

and the derivatives

$$\begin{aligned} \dot{x} &= -0.000011, \\ \dot{y} &= 0.002946, \\ \dot{z} &= -0.003570. \end{aligned} \tag{10}$$

The existence of homoclinic orbits implies the destruction of periodic orbits when the self-growth rate for prey $\tilde{x}$ is increased according to the scenario described by Gaspad et al. [24,26]. Moreover, when such an orbit is observed, the time evolution of the species is rather characteristic (Fig. 13). The food chain remains near the equilibrium during a significant interval and large eruption of the population can be observed. The length of the 'static' phase depends on the reinjection of the trajectory in the neighborhood of the point p. Although determinist, such a time interval is too sensitive to initial conditions to be efficiently predicted. From a practical point of view, abrupt eruptions of the species appear apparently in a random manner.

4. Conclusion

A fairly realistic three-species food chain model based on the Leslie–Gower scheme has been investigated. It has been shown that the time evolution of different species can be chaotic. A type-I intermittency has also been observed. It suggests that, without any external factor such as epidemic or weather conditions, populations of preys and predators may evolve regularly and then, abruptly start to evolve in a chaotic manner. After a given time duration, the population evolves regularly again.

When the growth-rate of the generalist predator is large enough, a bistability can be observed, i.e., two different attractors with their respective attraction basins may co-exist. In such a case, an epidemic or significant climate change may provoke a transition from one dynamical behavior to another. For instance, the time evolution of the populations can be regular and become irregular after an epidemic, or vice versa.

Another particular behavior is when the trajectory of the time evolution of the system describes a homoclinic orbit. In such a case, the populations are almost constant during a finite time interval and, suddenly, a large oscillation is observed. Since the time duration of such a 'nearly static' phase is highly dependent on initial conditions, the large oscillations seem to appear randomly.

References

[1] Hastings A, Powell T. Chaos in three-species food chain. Ecology 1991;72:896–903.
[2] Rinaldi SR, Muratori S, Kuznetsov Y. Multiple attractors, catastrophies and chaos in seasonally perturbed predator prey communities. Bull Math Biol 1993;55:15–35.
[3] Klebanoff A, Hastings A. Chaos in three-species food chain. J Math Biol 1994;32:427–51.
[4] McCann K, Yodzis P. Biological conditions for chaos in a three-species food chain. Ecology 1994;75:561–4.
[5] Kuznetsov YUA, Rinaldi S. Remarks on food chain dynamics. Math Biosci 1996;134:1–33.
[6] Upadhyay RK, Iyengar SRK, Rai V. Stability and complexity in ecological systems. Chaos, Solitons & Fractals 2000;11(4):533–42.
[7] Aziz-Alaoui MA. Stability and chaos in a realistic three species food chain model. SIAM J Appl Math; 2000 [submitted].
[8] Gilmore R. Topological analysis of chaotic dynamical systems. Rev Mod Phys 1998;70(4):1455–529.
[9] Mindlin GB, Solari HG, Natiello MA, Gilmore R, Hou XJ. Topological analysis of chaotic time series data from the Belousov–Zhabotinski reaction. J Nonlinear Sci 1991;1:147–73.
[10] Letellier C, Dutertre P, Maheu B. Unstable periodic orbits and templates of the Rössler system: toward a systematic topological characterization. Chaos, Solitons & Fractals 1995;5(1):271–82.
[11] Hamshi IL, Hamson L, Henttonen H. Specialist predators, generalist predators and the microtine rodent cycle. J Animal Ecol 1991;60:353–67.
[12] Upadhyay RK, Jyengar SRK, Rai V. Chaos: an ecological reality. Int J Bifurc Chaos 1998;8(6):1325–33.
[13] Jorgensen SE. Handbook of environmental data and ecological parameters. New York: Pergamon Press; 1979. p. 142–216.
[14] Cvitanović P. Periodic orbits as the skeleton of classical and quantum chaos. Physica D 1991;51:138–51.
[15] Collet P, Eckmann JP. Iterated maps on the interval as dynamical systems. In Jaffe A, Ruelle D, editors. Progress in physics. Boston: Birkhäuser; 1980.
[16] Pomeau Y, Manneville P. Intermittent transition to turbulence in dissipative dynamical systems. Commun Math Phys 1980;74:189–97.
[17] Schuster HG. Deterministic chaos. Weinheim: VCH; 1995.
[18] Hall T. Weak universality in two-dimensional transitions to chaos. Phys Rev Lett 1993;71(1):58–61.
[19] Feigenbaum MJ. Quantitative universality for a class of nonlinear transformation. J Statist Phys 1978;19(1):25–52.
[20] Coullet P, Tresser C. Itérations d'endomorphismes et groupe de renormalisation. Journal de Physique, Colloque C5, supplément au 1978;8(39):C5–25.
[21] Hao Bai Lin. Elementary symbolic dynamics and chaos in dissipative systems. Singapore: World Scientific Publishing; 1989.
[22] Dutertre P. Caractérisation des attracteurs étranges par la population d'orbites périodiques. Ph.D. dissertation, Université de Rouen, France; 1995.
[23] Dawson SP, Grebogi C, Kan I, Koçak H. Antimonotonicity: inevitable reversals of period-doubling cascades. Phys Lett A 1992;162:249–54.
[24] Gaspard P, Nicolis G. What can we learn from homoclinic orbits in chaotic dynamics. J Statist Phys 1983;31(3):499–518.
[25] Letellier C. Caractérisation topologique et reconstruction d'attracteurs étranges. Ph.D. dissertation, Université de Paris VII; 1994.
[26] Gaspard P, Kapral R, Nicolis G. Bifurcation phenomena near homoclinic systems: a two parameter analysis. J Statist Phys 1984;35(5/6):697–727.
[27] Sil'nikov LP. The existence of a denumerable set of periodic motions in four-dimensional space in an extended neighborhood of a saddle-focus. Dokl Akad Nauk SSSR 1967;1(172):54–8.